Perspective

Molecular Determinants of Current Blockade Produced by Peptide Transport Through a Nanopore

Jingqian Liu and Aleksei Aksimentiev*

Cite This: *ACS Nanosci. Au* 2024, 4, 21−29

Read Online

ACCESS | Metrics & More | Article Recommendations

ABSTRACT: The nanopore sensing method holds the promise of delivering a single molecule technology for identification of biological proteins, direct detection of post-translational modifications, and perhaps de novo determination of a protein's amino acid sequence. The key quantity measured in such nanopore sensing experiments is the magnitude of the ionic current passing through a nanopore blocked by a polypeptide chain. Establishing a relationship between the amino acid sequence of a peptide fragment confined within a nanopore and the blockade current flowing through the nanopore remains a major challenge for realizing the nanopore protein sequencing. Using the results of all-atom molecular dynamics simulations, here we compare nanopore sequencing of DNA with nanopore sequencing of proteins. We then delineate the factors affecting the blockade current modulation by the peptide sequence, showing that the current can be determined by (i) the steric footprint of an amino acid, (ii) its interactions with the pore wall, (iii) the local stretching of a polypeptide chain, and (iv) the local enhancement of the ion concentration at the nanopore constriction. We conclude with a brief discussion of the prospects for purely computational prediction of the blockade currents.

KEYWORDS: protein sequencing, nanopores, ionic current, molecular dynamics, current blockade, translocation, post-translational modifications
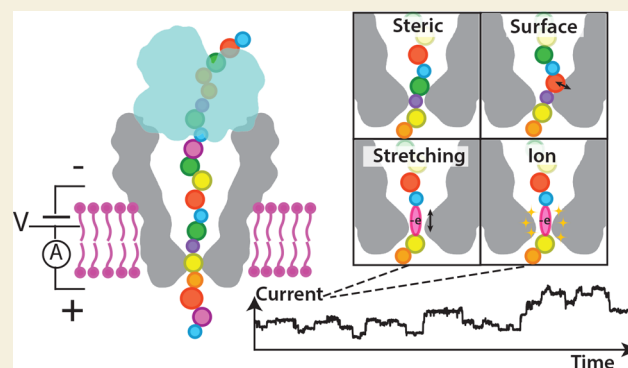
Reading the amino acid sequence of individual proteins with high precision and throughput holds the promise of delivering the most detailed portrait of a biological cell.[1] In the absence of natural mechanisms to copy, read, or transcribe protein sequences, abiological approaches to protein sequencing have taken a lead.[2] While improving conventional protein sequencing methods, such as Edman degradation[3] and mass spectrometry,[4] has its merits, the ultimate advances may come from nanopore sequencing,[5] Figure 1a, a single molecule sensing tehcnique that, in the field of DNA sequencing, has matured from a pipe dream to commercial enterprise.[6]

In a typical nanopore experiment, a nanopore is embedded in a thin, electrically insulating membrane separating a volume of electrolyte solution into two compartments connected by the nanopore. Electric field is applied across the membrane using two electrodes placed at the opposite sides of the membrane. In contrast to conventional gel electrophoresis, where the electric field is evenly distributed over the macroscopic distance between the electrodes, in a nanopore experiment, the field is focused to the vicinity of the nanopore.[7] The electric field extending from the nanopore entrance can bring a charged analyte molecule from the solution to the nanopore and then push the molecule through the nanopore to the other side of the membrane, transiently

reducing the ionic current flowing through the nanopore. Such ionic current blockades are measured experimentally and used to determine the chemical structure of the molecule.

Early measurements of nanopore transport found DNA molecules to pass through the nanopores too quickly for the DNA sequence to be determined with a single nucleotide resolution from the blockade current signatures.[8,9] The solution to the DNA speeding problem came in the form of a DNA binding enzyme, which is too large to pass through the nanopores.[10] In addition to serving as a translocation stopper, the biological enzyme can perform a host of useful (for DNA sequencing) functions, most importantly to thread the DNA polymer through the nanopore in single nucleotide steps and to unzip double-stranded DNA. Combining the stepwise translocation of DNA enabled by the biological enzyme with an improved nanopore, MspA,[11] which confines only a few
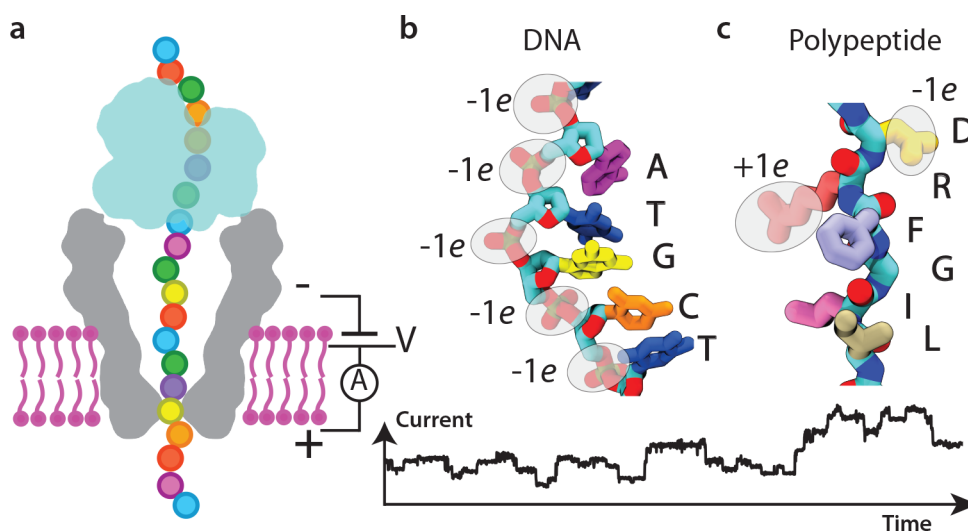
Figure 1. Nanopore sequencing of nucleic acids and proteins. (a) Simplified schematics of a typical nanopore sequencing experiment. A biological nanopore is embedded in a thin insulating membrane. A strand of a biopolymer—a nucleic acid or a polypeptide—is threaded through the nanopore. A transmembrane voltage is applied across the membrane, generating the flow of ions through the partially blocked nanopore. The motion of the biopolymer through the nanopore is controlled by the tug of war of the transmembrane electric field and the pull of a biological molecular motor. The ionic current fingerprint produced by the displacement of the biopolymer chain through the nanopore is used to decipher the nucleic or amino acid sequence of the biopolymer. (b) Representative fragment of a DNA strand with DNA bases shown in different colors. (c) Fragment of a polypeptide chain containing a representative set of amino acids. Symbol e denotes the charge of a proton.

DNA nucleotides at a time in its constriction, has made nanopore sequencing of DNA possible.[12,13]

Efforts to adopt the concept of nanopore DNA sequencing to protein sequencing have been ongoing starting with the pioneering work that used either an unfoldase motor[14] or a DNA tag[15] to thread and unfold native proteins through a biological nanopore α-hemolysin. But, in comparison to DNA sequencing, nanopore sequencing of proteins faces multiple challenges that stem from the chemical structure of a polypeptide chain. Under physiological conditions, a DNA strand carries a uniform electric charge of one electron per each phosphate backbone of its nucleotides, Figure 1b. A polypeptide's backbone, however, is electrically neutral and the charge of a polypeptide chain is dictated by the charge of its side chains, Figure 1c. Thus, the force of the electric field alone may not be sufficient to capture and unidirectionally transport a polypeptide chain through a nanopore. Multiple solutions have been described to address this problem, which includes the use of electro-osmotic[16,17] or dielectrophoretic[18] forces, or changing the charge of the polypeptide by either bathing a protein in a detergent solution,[19−21] changing pH of the solution,[22] and/or appending the proteins with charged tags.[15,21,23] Please see recent reviews for a complete account of the literature.[2,24,25]

Another challenge—the main topic of this article—relates to identifying individual amino acids from the blockade current signature that a peptide strand makes when passing through a nanopore. Reading the DNA sequence boils down to identifying one of the four canonical DNA bases. Although the differences among the bases are small, Figure 1b, the similar chemical structure of the bases alleviates, to some degree, complications related to differential interactions with the nanopore surface, which as we show below, is not the case for polypeptides.

More importantly, protein sequencing requires identification of the twenty amino acids, which can be done for individual amino acids attached to the same polypeptide carrier[26] or

transiently bound to a modified nanopore,[27] but becomes a formidable challenge in the context of a random sequence background. Thus, a protein nanopore that confines four nucleotides at a time can produce current levels from $4^4 = 256$ possible nucleotide combinations, i.e., k-mers. The same nanopore will confine about seven amino acids at a time and thus produce a total of $20^7 = 1.28 \times 10^9$ current levels. Taking into account the abundance and diversity of posttranslational modifications,[28] the latter number can be astronomically higher.

Below, we use the results of all-atom molecular dynamics (MD) simulations to describe four factors that determine a sequence-specific blockade current produced by a peptide transport through a nanopore. We show that, in addition to a volume exclusion mechanism seen in the case of DNA,[29] the blockade current is determined by at least three additional effects that stem from the heterogeniety of a polypeptide chain structure. While our work does not provide a solution to resolving the astronomical number of possible amino acid combinations that one would expect to encounter in de novo protein sequencing, it provides a framework for designing singal processing tools aiming at protein identification, detection of mutations, and post-translational modifications.

NANOPORE SEQUENCING OF DNA VERSUS NANOPORE SEQUENCING OF PROTEINS

Prior to describing the factors affecting the blockade current from peptide translocation, it is instructive to compare nanopore sequencing of DNA with nanopore sequencing of proteins under ideal circumstances, when both carry uniform negative charge. For the purpose of such comparison, we constructed a simulation system containing a DNA strand threaded through a truncated version of an MspA nanopore, a computationally efficient model that retains all essential properties of a full length MspA system.[29,30] Upon embedding the nanopore/DNA complex within a patch of a lipid membrane and solvating the system with 0.4 M KCl
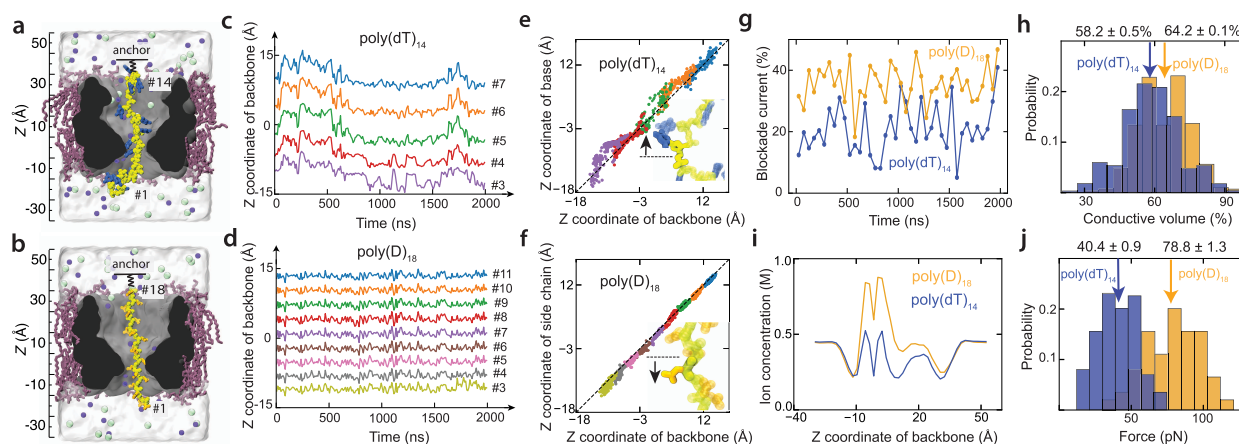
Figure 2. Nanopore sequencing of DNA versus nanopore sequencing of a charged polypeptide. (a,b) All-atom models of a reduced-length MspA (gray) containing a DNA (panel a) or a polypeptide (panel b) strand. A lipid membrane (orchid) separates the solvent volume (semitransparent surface) into two compartments; lime and purple spheres represent chloride and potassium ions, respectively. The top end of each strand is restrained using a harmonic potential, representing the action of an enzyme. (c,d) Backbone coordinates of individual DNA nucleotides (panel c) or amino acids (panel d) as a function of time during MD simulations of the systems shown in panels a and b under a 180 mV bias. The coordinate axis is defined in panels a and b. (e,f) Nucleobase (panel e) or side chain (panel f) coordinate versus backbone coordinate of individual nucleotides or amino acids, respectively, extracted from the MD simulations. (g) Simulated blockade currents. Each data point represents a 50 ns average of 20 ps sampled instantaneous current. (h) Normalized distribution of the relative conductive volume in the poly(dT)$_{14}$ and poly(D)$_{18}$ systems. The relative conductive volume is defined as the number of bulk water molecules located within the MspA constriction divided by the number of such molecules in the absence of the analyte. (i) Ion concentration profiles along the pore axis in the poly(dT)$_{14}$ and poly(D)$_{18}$ systems. (j) Normalized histograms of the effective force acting on the poly(dT)$_{14}$ and poly(D)$_{18}$ strands under a 180 mV bias. The effective force was calculated by multiplying the displacement of the top end of each strand from its restrained coordinate by the spring constant of the restrain.

electrolyte, the system was simulated for 2 μs under a 180 mV transmembrane voltage while a harmonic potential restrained the position of the top DNA nucleotide, reproducing the anchoring action of a biological enzyme, Figure 2a. A second system was built and simulated under identical conditions featuring a polypeptide chain, Figure 2b. Both strands contained a chemically uniform and electrically charged sequence: poly(dT)$_{14}$ in the case of the DNA and poly(D)$_{18}$ in the case of the polypeptide. The lengths of the biopolymers were chosen to span, approximately, a similar distance along the nanopore axis under the same applied bias.

Figure 2c,d plots the location of each monomer during a 2 μs simulation at 180 mV. The monomers of both biopolymers are seen to undergo stochastic displacement relative to the MspA constriction (located at $z = 0$). The displacement in both cases is coherent among the monomers of the same strand, which we attribute to their electric charge. Much less coherence is expected for a heterogeneous sequence peptide, as some amino acids do not carry a net electric charge and may interact specifically with the nanopore surface. The amplitude of the stochastic displacement, computed as the root mean squared displacement, is 2.3 Å for the DNA, four times larger than the average stochastic displacement of the polypeptide, 0.6 Å, which we attribute to the higher tension in the latter strand. Finally, the spacing among the consecutive monomers is noticeably greater in the DNA strand: 1.4 nucleotides are confined, on average, within the 8 Å length of the nanopore constriction, whereas 2.6 amino acid residues are confined within the same nanopore volume. The average intermonomer distance along the nanopore axis is thus 5.5 Å and 3.1 Å in the nanopore, which compares well with the 6.8 Å and 3.5 Å distances extracted from the respective chemical structures.

Although both strands are negatively charged, they adopt statistically different conformations within the nanopore constriction. Thus, the backbone of a thymine nucleotide is

located, on average, 1.0 Å lower than the DNA base of the same nucleotide, Figure 2e, whereas the backbone of an aspartic amino acid is located, on average, 0.7 Å higher than its side chain, Figure 2f. These systematic differences in the local structure of the biopolymers at the nanopore constriction are caused by the differential localization of the electrical change within a nucleotide or a polypeptide monomer, Figure 1b,c.

Knowing the coordinates of each atom in an MD simulation, we can compute the ionic current flowing through the nanopore from the instantaneous displacement of the ions.[31,32] Such raw current trances, however, are very noisy as they account for the thermal (stochastic) displacement of ions.[33] Averaging the instantaneous currents in 50 ns blocks and then dividing each block-average value by the average open pore current (determined from an additional simulation) reveals how the simulated blockade current changes over the course of the MD trajectory and how it depends on the biopolymer type, Figure 2g. In general agreement with experiment, the relative blockade current through MspA is about 2-fold larger when the pore is blocked by a charged polypeptide strand,[34] in comparison to a DNA strand under similar conditions.[12] Such a large difference cannot be fully explained by the difference in the steric footprints of the monomers, as the respective conductive volume of the nanopore constriction differs by only ~10%, Figure 2h. Hereafter, a steric footprint of a molecule refers to the molecule's ability to reduce the number of bulk-like water molecules when placed in a solution and, in practice, means the volume occupied by the molecule and its first solvation shell. We attribute the remaining difference of the blockade currents to the strong enhancement of ion concentration in the nanopore constriction, Figure 2i, caused by the higher charge density of the polypeptide strand. The difference in the local charge density can largely account for the 2-fold difference in
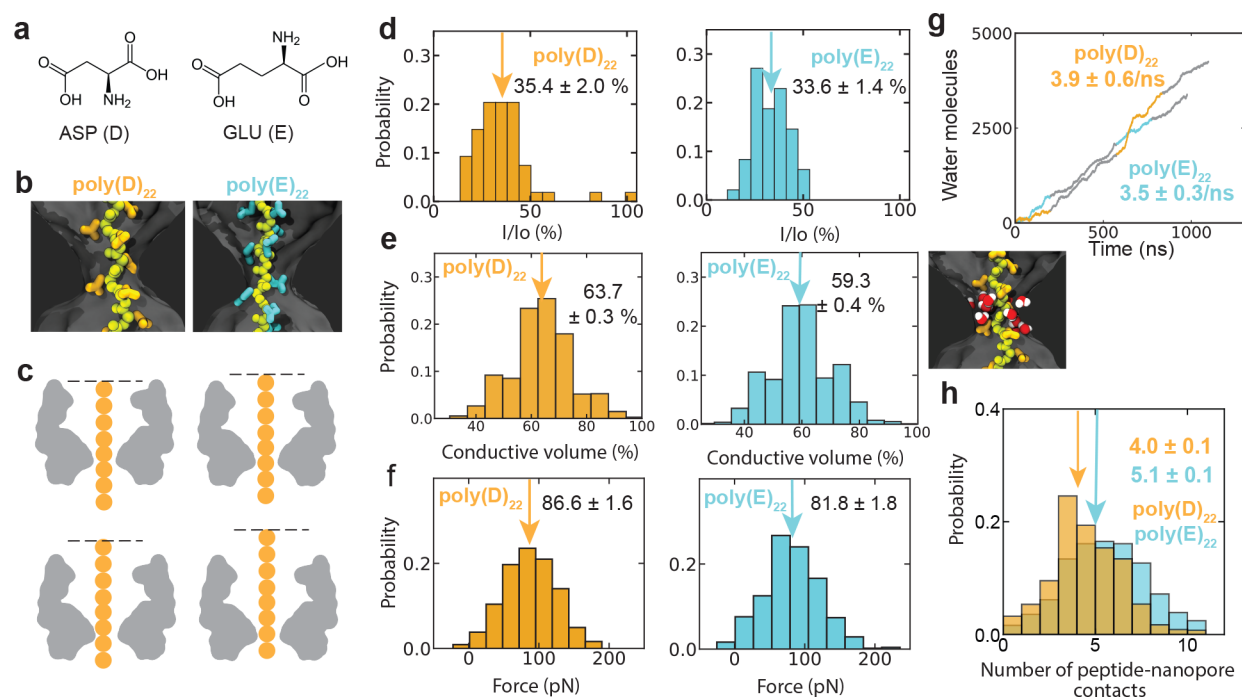
Figure 3. Blockade current is modulated by a steric footprint of the amino acid. (a) Chemical structures of aspartic (left) and glutamic (right) amino acids. (b) Closed-up view of the poly(D) and poly(E) peptides stretched through the constriction of MspA. (c) Schematic representation of multicopy sampling of the simulated blockade current. Each system differs from another by the location of the anchor potential applied to the top amino acid. (d−f) Normalized distribution of the simulated blockage current, conductive volume and the effective force in poly(D)$_{22}$ and poly(E)$_{22}$ systems. The blockade current histograms were constructed using four independent trajectories ∼1.3 μs in their total duration and 20 ns block averages of the instantaneous current. (g) Number of water molecules that passed through the nanopore constriction versus simulation time. For each system, data from four independent simulations are shown using alternating colors. The mean value and the standard error were calculated using 50 ns block averages. (h) Statistics of peptide−nanopore constants. A contact was defined as having a non-hydrogen atom of the peptide and an atom of the nanopore separated by less than 3 Å. The average value and the standard error were calculated using 10 ns block averages.

the effective force[35] applied to the strands by the electric field in the nanopore, Figure 2j.

Determinants of Current Blockade: Steric Exclusion

Previously, we have shown that, in the case of DNA translocation, the ionic current blockade is determined by the conductive volume of the nanopore constriction and that the nucleotide sequence of the DNA modulates the blockade current by altering the conductive volume of the nanopore.[29] To determine if the same steric exclusion mechanism is at play in the peptide translocation case, we examined the current blockades produced by two uniformly charged polypeptides, poly(D)$_{22}$ and poly(E)$_{22}$, that differ solely by the presence of a single methylene group in each amino acid side chain, Figure 3a,b. In order to enhance sampling, we conducted four replica simulations for each system, anchoring the top residue of the strands at different locations above the nanopore, Figure 3c.

Figure 3d plots the distribution of the relative blockade current obtained from the simulations of the poly(D)$_{22}$ and poly(E)$_{22}$ systems. The polypeptide chain containing larger amino acids (glutamic acid, E) is seen to block the current more, with the blockade current difference being about 6% of the absolute current value. Similar magnitude difference is observed when comparing the relative conductive volume of the nanopore constriction occupied by the poly(D) and poly(E) strands. Thus, the addition of a single methylene group to the side chain of an amino acid produces a small yet measurable decrease of the blockade current and the magnitude of such a decrease is quantitatively similar to the reduction of the nanopore conductive volume. Thus, steric

exclusion determines the blockade current not only in the so-called whole molecule sensing measurements,[26,36] but also in strand sequencing of a polypeptide, a conjecture echoed by recent experiments.[37,38]

The steric footprint is found to introduce a small yet statistically significant difference in the effective force acing on the polypeptides, with the bulkier side chains reducing the effective force, Figure 3f. The difference cannot be attributed to the drag of the electro-osmotic flow[35] as we did not observe a statistically significant difference in the average water flux through the nanopores, Figure 3g. We attribute the effective force difference to direct interactions between the polypeptide and the nanopore, Figure 3h, which was previously shown to considerably affect the effective force on DNA in a solid-state nanopore.[39] Note that the effective force on poly(D)$_{22}$, Figure 3f, is only marginally higher than on poly(D)$_{18}$, Figure 2j, because the majority of the electric field is focused at the nanopore constriction.

Determinants of Current Blockade: Interaction with the Nanopore Surface

A straightforward approach to controlling the nanopore transport of a charged polypeptide is to chemically link the polypeptide to a fragment of DNA and then use the already established methodology of stepping DNA through a nanopore with the help of a DNA processing enzyme.[34,40] This approach has been demonstrated in the proof-of-concept experiments,[34] where three polypeptide chains differing by a single amino acid substitution were pulled against the force of the electric field using a helicase motor, Figure 4a. The resulting ionic current
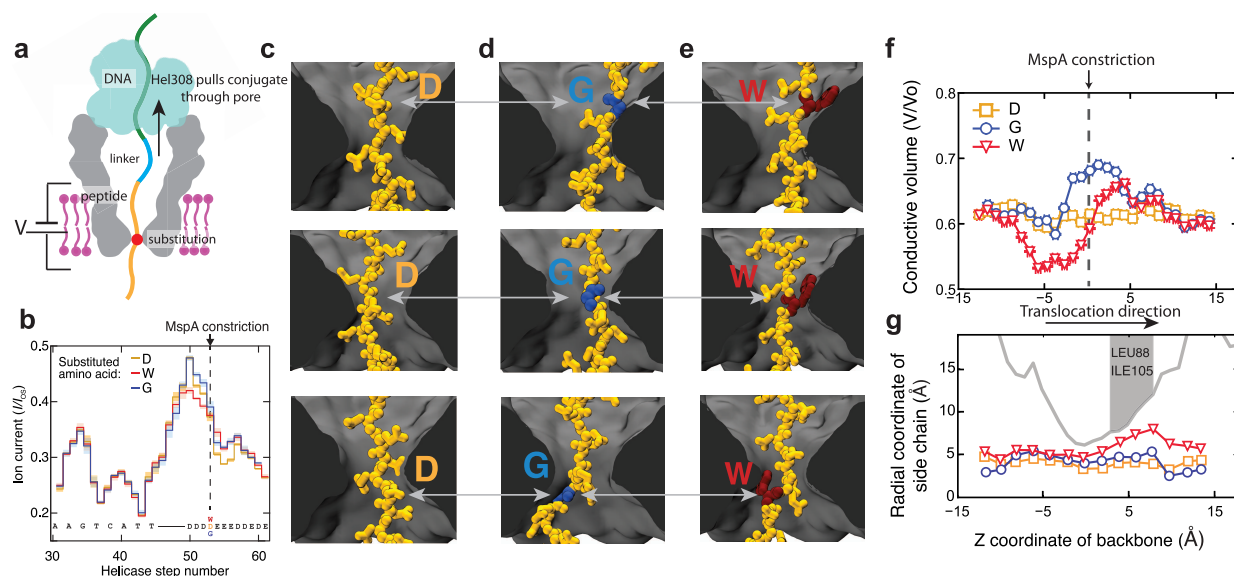
Figure 4. Specific interactions between peptide amino acids and the nanopore can modulate the blockade current. (a) Schematics of an experimental system for measuring ionic current signatures of single amino acid substitutions. (b) Experimentally recorded blockade currents resulting from a helicase-assisted nanopore motion of three DNA−peptide constructs differing by a single amino acid substitution. (c−e) Sequence of snapshots illustrating upward displacement (from bottom to top) of three polypeptide strands through the MspA constriction. The locations of the single amino acid substitution are highlighted by the arrows. (f) Fraction of nanopore constriction volume available for ion transport. Vertical and horizontal error bars denote standard errors and standard deviations, respectively. (g) Radial center-of-mass coordinate of the substituted residue side chain versus the center-of-mass coordinate of the residue's backbone. The radial coordinate was computed relative to the symmetry axis of the MspA nanopore. The gray line shows the local radius of the MspA nanopore. The annotated residues exhibit strong interactions with the W substitution. Panels b, f, and g are adapted with permission from ref 34, Copyright 2021 American Association for the Advancement of Science.
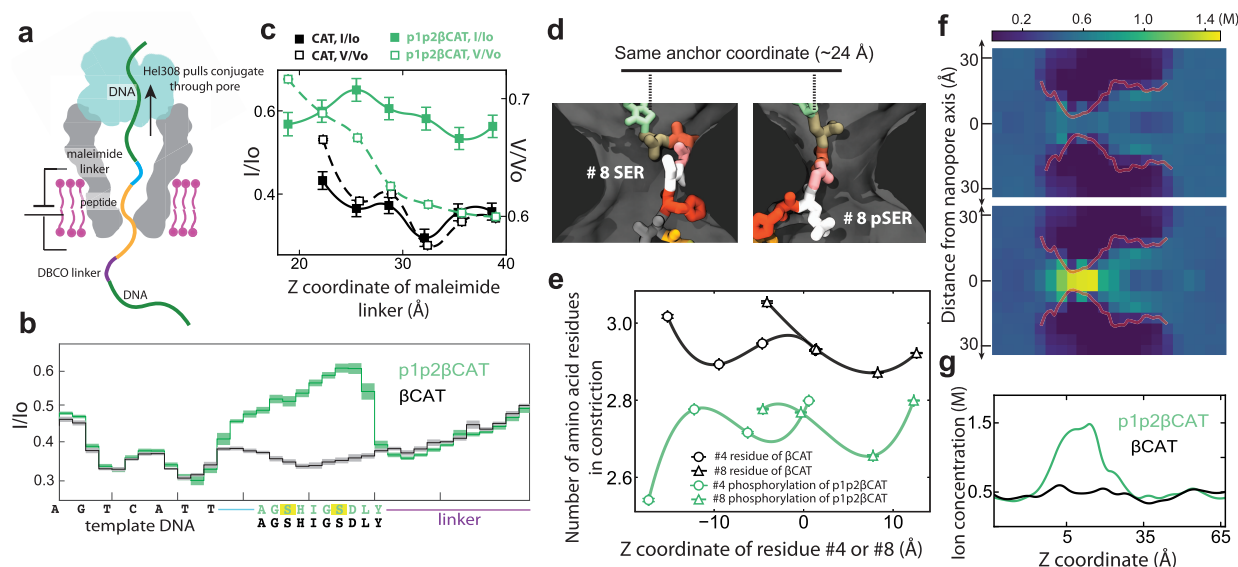
Figure 5. Peptide stretching and ion congregation enable detection of phosphorylation. (a) Schematics of an experimental system for measuring ionic current signatures of amino acid phosphorylation.[23] (b) Experimentally recorded blockade currents resulting from a helicase-assisted motion of two DNA−peptide−DNA constructs differing by the phosphorylation state of the two serine residues (highlighted in yellow).[23] Adapted with permission from ref 23, Copyright 2023 Springer Nature America. (c) Simulated blockade current (left axis, solid lines) and relative conductive volume (right axis, dashed lines) as a function of the linker position. (d) Representative conformations of the nonphosphorylated (left) and phosphorylated (right) peptide held by the linker anchor located the same distance above the nanopore constriction. (e) Number of peptide residues within the 8 Å constriction of the MspA nanopore versus the z coordinate of the phosphorylated residue. The average number of peptide within the constriction and the standard error were computed using 6.6 Å bins along the z axis. (f) Heatmap of local KCl concentration in the MspA nanopore blocked by the nonphosphorylated (top) and phosphorylated (bottom) variants of the peptide. The map was constructed using 4 Å bins along the pore axis and 5 Å bins normal to it, and averaged radially with respect to the nanopore axis and over the respective MD trajectories. (g) Local concentration of KCl along the symmetry axis of the MspA nanopore blocked by the two peptides.

blockades, Figure 4b, showed considerable differences near the expected locations of the single amino acid substitutions,

however, the character of the current modulations was found to depend on the type of the amino acid substitution in a

nontrivial manner: while the smaller amino acid, glycine (G) increased the ionic current relative to the baseline amino acid type (D), the largest amino acid—tryptophan (W)—could both decrease or increase the current, depending on its putative location relative to the nanopore constriction.

Three sets of multicopy MD simulations have determined the molecular cause of such puzzling ionic current dependence. The displacement of a mixed-sequence (DE) polypeptide, Figure 4c, was found to produce no noticeable changes of the conductive volume of the nanopore, Figure 4f, and, hence, of the ionic current.[34] The passage of a glycine substitution through the nanopore constriction, Figure 4c, was accompanied by the transient increase of the conductive volume, Figure 4f, and the ionic current,[34] in accordance with the steric exclusion mechanism. For the tryptophan substitution, however, the conductive volume was first observed to decrease but then transiently increase as the substitution exists the nanopore constriction, Figure 4f. Further analysis showed that this transient increase is correlated with direct (hydrophobic) interaction of the tryptophan residue to the surface of the nanopore above the constriction, Figure 4g. This interaction reduced the effective footprint of the polypeptide in the nanopore by reducing the number of water molecule exposed to the combined surface of the nanopore and the peptide, similar to the effects previously reported for DNA[41] and protein[42] systems. Thus, specific interactions between the residues of the nanopore surface and the residues of the peptide can modulate the blockade current by altering the conductive volume of the nanopore.

Determinants of Current Blockade: Stretching and Ion Congregation

The vast majority of biological peptides are heterogeneous with regard to their local hydrophobicity and electrical charge. This heterogeneity becomes even more diverse when taking into account a large library of possible post-translational modifications.[28] One common modification is phosphorylation, which changes the charge of a modified amino acid.

Nanopore detection of peptide phosphorylation has become possible in the broader context of nanopore sequencing by chemically linking both ends of a target peptide to two DNA fragments and using a helicase motor to move the peptide in discrete steps through the nanopore constriction,[23] Figure 5a. These experiments specifically examined βCAT peptides, which are of immunological significance to several health conditions including cancers, Alzheimer's, and heart diseases.[28] Experimentally, phosphorylation of the two serine residues within the βCAT sequence was found to produce a pronounced increase of the blockade current, in comparison to the nonphosphorylated peptide variant, Figure 5b. This is a counterintuitive result as the addition of a phosphate group increases the steric footprint of the modified residue, which is expected to decrease the blockade current.

We have identified the molecular mechanisms responsible for such a dramatic (almost 2-fold) increase of the ionic current upon phosphorylation. Two sets of multicopy MD simulations of a reduced-length MspA system each containing either variant of the βCAT peptide reproduced the experimentally measured difference in the blockade current, Figure 5c. In such simulations, the peptide's location was controlled by restraining the coordinates of the maleimide linker above the nanopore constriction, allowing the peptide to adopt its preferred conformation within the nanopore.

First, we noticed that placing a negatively charge phosphate group on a serine residue produced pronounced stretching of the peptide in the nanopore constriction, in comparison to the conformation of the nonphosphorylated peptide anchored at the same location above the nanopore, Figure 5d. The stretching effect was consistent among all replica simulations and robust regarding the choice of the phosphorylated residue, i.e., at position 4 or 8 of the peptide, Figure 5e. The stretching was seen to increase the conductive volume of the nanopore constriction, Figure 5c, and thereby the ionic current via the steric exclusion mechanism. Stretching alone, however, was not sufficient to explain the sustained level of higher current seen for the phosphorylated peptide (top trace in Figure 5c), as the additional steric footprint of the phosphorylated group compensated the conductive volume increase due to stretching when the group entered the nanopore constriction.

Further analysis of our MD trajectories showed that the local addition of the electrical charge by the phosphorylation markedly increases the local concentration of cations within the nanopore, Figure 5f,g. Tripling the number of the charge carries within the bottleneck to the ion passage, i.e., the nanopore constriction, locally increases its conductivity and, hence, the overall ionic current. Thus, both effects—local stretching of the peptide and local enhancement of ion concentration—contribute to the ionic current enhancement in the specific scenario depicted in Figure 5. We note, however, that the two effects do not have to occur simultaneously, as peptide stretching can be produced by external factors, such as a peptide unfoldase pulling the peptide strand through a nanopore,[38] whereas ion current enhancement can occur independently of stretching when a charged amino acid flanked by uncharged residues passes through the nanopore constriction.

■ OUTLOOK

We have described four factors affecting the blockade current produced by peptide transport through nanopores. Our description is, of course, not complete and we expect further work to discover additional mechanisms, which could be related, for example, to interactions between the amino acids within a polypeptide strand (akin to base-stacking in DNA) or partial dehydration of the nanopore volume. While we expect the all-atom MD method to continue provide invaluable insights into the microscopic mechanisms enabling amino acid identification, using this method to predict the blockade current for 10^9 possible permutations of amino acid residues will remain impractical for the forceable future. Simpler computational methods[43−45] or empirical models,[38] informed by the outcome of brute force all-atom simulations, will have to be developed to provide fast and accurate estimate of the blockades current and used for training of the amino acid caller algorithms. Among the most anticipated advances in the methodology of computational modeling of the blockade currents are algorithms enabling computationally efficient and statistically sound sampling of polypeptide conformations under nonequilibrium conditions of the nanopore measurement and precise continuum models of ionic current capable of handling highly nonuniform distributions of ions within the nanopore volume. The advent of such methods will allow the decomposition of the ionic current prediction problem into two independent computational tasks and will create conditions enabling purely in silico machine learning of the sequence−current relationships.

■ METHODS

General MD Methods

Unless specified otherwise, all MD simulations were carried out using NAMD2[46] under periodic boundary conditions and a time step of 2 fs. The CHARMM36 force field[47,48] was used to describe proteins, DNA, lipid bilayer membranes,[49] water,[50] and ions[51] along with the CUFIX corrections applied to improve description of charge−charge interactions.[52−54] RATTLE[55] and SETTLE[56] algorithms were applied to covalent bonds that involved hydrogen atoms in protein and water molecules, respectively. The particle mesh Ewald (PME)[57] algorithm was adopted to evaluate the long-range electrostatic interaction over a 1 Å-spaced grid. Van der Waals interactions were evaluated using a smooth 10−12 Å cutoff. Bonded and short-ranged nonbonded interactions were evaluated every time step whereas long-range nonbonded interactions were evaluated every third time step. The Nose-Hoover Langevin piston pressure control[58] was used to maintain the pressure of the system at 1 atm by adjusting the system's dimension. Langevin thermostat[59] was applied to all heavy atoms of the lipid membrane with a damping coefficient of 1 ps^{-1} to maintain the temperature of the system at 295 K. The simulations performed using the D. E. Shaw Research supercomputer Anton2[60] employed a set of parameters equivalent to those listed above, except for the use of the Nosé-Hoover thermostat[61] and the k-space Gaussian split Ewald method[62] for calculations of the electrostatic interactions.

All-Atom Models and Simulations of poly(dT)$_{12}$ and poly(D)$_{18}$ MspA Systems

All MspA systems were built using a reduced-length model of MspA that included residues 75−120 of the full-length protein.[30] Each system contained approximately 40000 atoms and included a 6.5 × 6.5 nm^2 patch of a palmitoyloleoyl phosphatidylethanolamine (POPE) bilayer solvated with 0.4 M KCl electrolyte. The simulations employed the M2-NNN variant of MspA,[63] where 32 aspartate residues were replaced by asparagine or arginine residues. The poly(dT)$_{14}$ strand was oriented to have its 3′ end in the MspA vestibule. The poly(D)$_{18}$ peptide was oriented to have its C-terminus in the MspA vestibule. After 2000 steps of energy minimization and 45 ns equilibration in the constant pressure (NPT) ensemble, each system was simulated for 2 μs in the constant volume (NVT) ensemble on Anton 2 under a 180 mV electrical bias applied across the membrane.[32] The C1′ atom of the 3′ terminus of the DNA and the C$_\alpha$ atom of the C-terminal residue of the peptide were restrained to the same anchor position using a harmonic potential of 1 kcal mol^{-1} Å^{-2} spring constant.

Multicopy Simulations of Charged Peptides Containing Single Amino Acid Substitutions

Initial systems each containing a polypeptides of one of the following amino acid sequences: C(D)$_{22}$ or C(E)$_{22}$, were built by combining the peptides with a reduced-length MspA, a DPhPC bilayer and 0.4 M KCl solution. In the main text, we refer to these polypeptides as poly(D)$_{22}$ and poly(E)$_{22}$ for brevity. Upon energy minimization and NPT equilibration, each system was simulated in the NVT ensemble under a 200 mV bias while the top residues of the peptide strand were moved by 6 Å up and down multiple times in a 400 ns simulation using the steered MD (SMD) protocol.[64] A representative ensemble of peptide conformations was used to initiate ionic current simulations under 200 mV, which were performed having the top residue of each peptide stationary restrained to its coordinate in the chosen instantaneous configuration. During these 200 ns simulations, the amino acid substitutions were located within 15 Å from the nanopore constriction. The details of the simulation protocols were described previously.[34]

MD Simulations of Phosphorylated Peptides in MspA

Each system contained a reduced-length MspA model, a peptide of the specified sequence, two chemical linkers covalently attached to the peptide's termini, a DPhPC bilayer and 0.4 M KCl solution. The systems were built using previous well-equilibrated peptide con-

formations and were re-equilibrated for 20 ns in the constant ratio NPT ensemble. The topologies and parameters of the DBCO-azide and maleimide linkers were generated using CHARMM General Force Field (CGenFF).[65,66] The charges of the atoms at the linker−peptide junction were adjusted by small amounts to produce an electrically neutral linker−peptide−linker conjugate. The conjugate was placed in a pre-equilibrated MspA system. Water molecules overlapping with the conjugate were removed. For each peptide variant, six systems were built differing by the location of the top (maleimide) linker. In all simulations, the phosphorus atom of that linker was harmonically restrained to an anchor located along the z axis 19 to 39 Å above the constriction. The z coordinate of the phosphorus atom of the bottom (DBCO-azide) linker was restrained as well but the atom was allowed to move within the x−y plane using a zero-velocity SMD protocol. The use of such restraints prevented the linkers from developing strong interactions with the nanopore, accounting for the action of the DNA fragments absent in our all-atom model. The simulations utilized a hydrogen mass repartitioning scheme, making it possible to use a time step of 4 fs.[67] Each 100 ns production simulation under a 180 mV bias was performed in the NVT ensemble with the system's dimensions set to the average values observed within the last 5 ns of the corresponding NPT equilibration.

Ion Current

Instantaneous ionic current was calculated as[31]

$$I(t) = \frac{1}{\Delta t l_z} \sum_{j=1}^{N} q_j (z_j(t+\Delta t) - z_i(t)),$$

(1)

where $z_j(t + \Delta t) - z_i(t)$ is the displacement of ion j along the z axis during the time interval $\Delta t = 20$ ps and q_j is the charge of ion j. To minimize the effect of thermal noise, the current was calculated within $l_z = 20$ Å slab centered at the nanopore constriction; the slab spanned the entire simulation system in the $x−y$ plane.

Conductive Volume

To calculate the fraction of the nanopore volume available to conduct ionic current, we first compute the average number of bulk-like water molecules confined within the 8 Å constriction of the MspA nanopore from an open-pore MD trajectory. Following that, we compute the conductive volume of the same nanopore section for MD trajectories of the MspA−DNA or MspA−peptide systems. The ratio of the two bulk water numbers defines the relative conductive volume of the nanopore constriction. In all conductive volume calculations, we define bulk-like water molecules as those located more than 2.5 Å away from any protein or DNA atom. Previously, we found this definition of the conductive volume to provide the best correlation with the blockade current produced by a DNA strand in MspA nanopore.[29]

■ AUTHOR INFORMATION

Corresponding Author

Aleksei Aksimentiev − *Department of Physics and Beckman Institute for Advanced Science and Technology, University of Illinois at Urbana−Champaign, Urbana, Illinois 61801, United States; Center for Biophysics and Quantitative Biology, University of Illinois at Urbana−Champaign, Urbana, Illinois 61801, United States;* ◉ orcid.org/0000-0002-6042-8442; Email: aksiment@illinois.edu

Author

Jingqian Liu − *Center for Biophysics and Quantitative Biology, University of Illinois at Urbana−Champaign, Urbana, Illinois 61801, United States; Beckman Institute for Advanced Science and Technology, University of Illinois at Urbana−Champaign, Urbana, Illinois 61801, United States*

Complete contact information is available at:
https://pubs.acs.org/10.1021/acsnanoscienceau.3c00046

Author Contributions

CRediT: **Jingqian Liu** formal analysis, investigation, visualization, writing-original draft, writing-review & editing; **Aleksei Aksimentiev** conceptualization, funding acquisition, project administration, supervision, writing-original draft, writing-review & editing.

Notes

The authors declare no competing financial interest.

■ ACKNOWLEDGMENTS

■ REFERENCES

(1) Tyers, M.; Mann, M. From Genomics to Proteomics. *Nature* **2003**, *422*, 193−197.

(2) Alfaro, J.; Bohländer, P.; Dai, M.; Filius, M.; Howard, C.; van Kooten, X.; Ohayon, S.; Pomorski, A.; Schmid, S.; Aksimentiev, A.; Anslyn, E.; Bedran, G.; Cao, C.; Chinappi, M.; Coyaud, E.; Dekker, C.; Dittmar, G.; Drachman, N.; Eelkema, R.; Goodlett, D.; et al. The Emerging Landscape of Single-molecule Protein Sequencing Technologies. *Nat. Methods* **2021**, *18*, 604−617.

(3) Edman, P. A. Method for the Determination of the Amino Acid Sequence in Peptides. *Arch. Biochem.* **1950**, *22*, 475−476.

(4) Steen, H.; Mann, M. The ABCs (and XYZs) of Peptide Sequencing. *Nat. Rev. Mol. Cell Biol.* **2004**, *5*, 699−711.

(5) Kasianowicz, J. J.; Brandin, E.; Branton, D.; Deamer, D. W. Characterization of Individual Polynucleotide Molecules Using a Membrane Channel. *Proc. Natl. Acad. Sci. U. S. A.* **1996**, *93*, 13770−13773.

(6) Deamer, D.; Akeson, M.; Branton, D. Three Decades of Nanopore Sequencing. *Nat. Biotechnol.* **2016**, *34*, 518−524.

(7) Wanunu, M.; Morrison, W.; Rabin, Y.; Grosberg, A. Y.; Meller, A. Electrostatic Focusing of Unlabelled DNA into Nanoscale Pores Using a Salt Gradient. *Nat. Nanotech.* **2010**, *5*, 160−165.

(8) Akeson, M.; Branton, D.; Kasianowicz, J. J.; Brandin, E.; Deamer, D. W. Microsecond Time-Scale Discrimination among Polycytidylic Acid, Polyadenylic Acid, and Polyuridylic Acid as Homopolymers or as Segments Within Single RNA Molecules. *Biophys. J.* **1999**, *77*, 3227−3233.

(9) Meller, A.; Nivon, L.; Brandin, E.; Golovchenko, J.; Branton, D. Rapid Nanopore Discrimination Between Single Polynucleotide Molecules. *Proc. Natl. Acad. Sci. U. S. A.* **2000**, *97*, 1079−1084.

(10) Cherf, G. M.; Lieberman, K. R.; Rashid, H.; Lam, C. E.; Karplus, K.; Akeson, M. Automated Forward and Reverse Ratcheting of DNA in a Nanopore at 5-Å Precision. *Nat. Biotechnol.* **2012**, *30*, 344−348.

(11) Faller, M.; Niederweis, M.; Schulz, G. E. The Structure of a Mycobacterial Outer Membrane Channel. *Science* **2004**, *303*, 1189−1192.

(12) Manrao, E. A.; Derrington, I. M.; Laszlo, A. H.; Langford, K. W.; Hopper, M. K.; Gillgren, N.; Pavlenok, M.; Niederweis, M.; Gundlach, J. H. Reading DNA at Single-Nucleotide Resolution with a Mutant MspA Nanopore and Phi29 DNA Polymerase. *Nat. Biotechnol.* **2012**, *30*, 349−353.

(13) Laszlo, A. H.; Derrington, I. M.; Ross, B. C.; Brinkerhoff, H.; Adey, A.; Nova, I. C.; Craig, J. M.; Langford, K. W.; Samson, J. M.; Daza, R.; Doering, K.; Shendure, J.; Gundlach, J. H. Decoding Long Nanopore Sequencing Reads of Natural DNA. *Nat. Biotechnol.* **2014**, *32*, 829−833.

(14) Nivala, J.; Marks, D. B.; Akeson, M. Unfoldase-Mediated Protein Translocation through an α-Hemolysin Nanopore. *Nat. Biotechnol.* **2013**, *31*, 247−250.

(15) Rodriguez-Larrea, D.; Bayley, H. Multistep Protein Unfolding During Nanopore Translocation. *Nat. Nanotech.* **2013**, *8*, 288−295.

(16) Gu, L. Q.; Cheley, S.; Bayley, H. Prolonged Residence Time of a Noncovalent Molecular Adapter, β-cyclodextrin, within the Lumen of Mutant α-hemolysin Pores. *J. Gen. Physiol.* **2001**, *118*, 481−493.

(17) Asandei, A.; Schiopu, I.; Chinappi, M.; Seo, C. H.; Park, Y.; Luchian, T. Electroosmotic Trap Against the Electrophoretic Force Near a Protein Nanopore Reveals Peptide Dynamics During Capture and Translocation. *ACS Appl. Mater. Interfaces* **2016**, *8*, 13166−13179.

(18) Tian, K.; Decker, K.; Aksimentiev, A.; Gu, L.-Q. Interference-Free Detection of Genetic Biomarkers Using Synthetic Dipole-Facilitated Nanopore Dielectrophoresis. *ACS Nano* **2017**, *11*, 1204−1213.

(19) Kennedy, E.; Dong, Z.; Tennant, C.; Timp, G. Reading the Primary Structure of a Protein with 0.07 nm³ Resolution Using a Subnanometre-Diameter Pore. *Nat. Nanotech.* **2016**, *11*, 968−976.

(20) Restrepo-Pérez, L.; John, S.; Aksimentiev, A.; Joo, C.; Dekker, C. SDS-assisted Protein Transport through Solid-state Nanopores. *Nanoscale* **2017**, *9*, 11685−11693.

(21) Yu, L.; Kang, X.; Li, F.; Mehrafrooz, B.; Makhamreh, A.; Fallahi, A.; Foster, J. C.; Aksimentiev, A.; Chen, M.; Wanunu, M. Unidirectional Single-file Transport of Full-length Proteins through a Nanopore. *Nat. Biotechnol.* **2023**, *41*, 1130−1139.

(22) Huang, G.; Voet, A.; Maglia, G. FraC Nanopores with Adjustable Diameter Identify the Mass of Opposite-charge Peptides with 44 Dalton Resolution. *Nat. Commun.* **2019**, *10*, 835.

(23) Nova, I. C.; Ritmejeris, J.; Brinkerhoff, H.; Koenig, T. J.; Gundlach, J. H.; Dekker, C. Detection of Phosphorylation Post-translational Modifications along Single Peptides with Nanopores. *Nat. Biotechnol.* **2023**, 1−5.

(24) Ying, Y.-L.; Hu, Z.-L.; Zhang, S.; Qing, Y.; Fragasso, A.; Maglia, G.; Meller, A.; Bayley, H.; Dekker, C.; Long, Y.-T. Nanopore-based Technologies Beyond DNA Sequencing. *Nat. Nanotech.* **2022**, *17*, 1136−1146.

(25) Wei, X.; Penkauskas, T.; Reiner, J. E.; Kennard, C.; Uline, M. J.; Wang, Q.; Li, S.; Aksimentiev, A.; Robertson, J. W.; Liu, C. Engineering Biological Nanopore Approaches toward Protein Sequencing. *ACS Nano* **2023**, *17*, 16369−16395.

(26) Ouldali, H.; Sarthak, K.; Ensslen, T.; Piguet, F.; Manivet, P.; Pelta, J.; Behrends, J. C.; Aksimentiev, A.; Oukhaled, A. Electrical Recognition of the Twenty Proteinogenic Amino Acids Using an Aerolysin Nanopore. *Nat. Biotechnol.* **2020**, *38*, 176−181.

(27) Wang, K.; Zhang, S.; Zhou, X.; Yang, X.; Li, X.; Wang, Y.; Fan, P.; Xiao, Y.; Sun, W.; Zhang, P.; Li, W.; Huang, S. Unambiguous Discrimination of All 20 Proteinogenic Amino Acids and Their Modifications by Nanopore. *Nat. Methods* **2023**.

(28) Xu, H.; Wang, Y.; Lin, S.; Deng, W.; Peng, D.; Cui, Q.; Xue, Y. PTMD: a Database of Human Disease-associated Post-translational Modifications. *Genomics Proteomics Bioinf* **2018**, *16*, 244−251.

(29) Bhattacharya, S.; Yoo, J.; Aksimentiev, A. Water Mediates Recognition of DNA Sequence *via* Ionic Current Blockade in a Biological Nanopore. *ACS Nano* **2016**, *10*, 4644−4651.

(30) Bhattacharya, S.; Derrington, I. M.; Pavlenok, M.; Niederweis, M.; Gundlach, J. H.; Aksimentiev, A. Molecular Dynamics Study of MspA Arginine Mutants Predicts Slow DNA Translocations and Ion Current Blockades Indicative of DNA Sequence. *ACS Nano* **2012**, *6*, 6960−6968.

(31) Aksimentiev, A.; Heng, J. B.; Timp, G.; Schulten, K. Microscopic Kinetics of DNA Translocation through Synthetic Nanopores. *Biophys. J.* **2004**, *87*, 2086−2097.

(32) Aksimentiev, A.; Schulten, K. Imaging α-Hemolysin with Molecular Dynamics: Ionic Conductance, Osmotic Permeability and the Electrostatic Potential Map. *Biophys. J.* **2005**, *88*, 3745−3761.

(33) Aksimentiev, A. Deciphering Ionic Current Signatures of DNA Transport through a Nanopore. *Nanoscale* **2010**, *2*, 468−483.

(34) Brinkerhoff, H.; Kang, A. S.; Liu, J.; Aksimentiev, A.; Dekker, C. Multiple Rereads of Single Proteins at Single−Amino Acid Resolution Using Nanopores. *Science* **2021**, *374*, 1509−1513.

(35) Luan, B.; Aksimentiev, A. Electro-Osmotic Screening of the DNA Charge in a Nanopore. *Phys. Rev. E* **2008**, *78*, 021912.

(36) Ensslen, T.; Sarthak, K.; Aksimentiev, A.; Behrends, J. C. Resolving Isomeric Posttranslational Modifications Using a Biological Nanopore as a Sensor of Molecular Shape. *J. Am. Chem. Soc.* **2022**, *144*, 16060−16068.

(37) Cardozo, N.; Zhang, K.; Doroschak, K.; Nguyen, A.; Siddiqui, Z.; Bogard, N.; Strauss, K.; Ceze, L.; Nivala, J. Multiplexed Direct Detection of Barcoded Protein Reporters on a Nanopore Array. *Nat. Biotechnol.* **2022**, *40*, 42−46.

(38) Motone, K.; Kontogiorgos-Heintz, D.; Wee, J.; Kurihara, K.; Yang, S.; Roote, G.; Fang, Y.; Cardozo, N.; Nivala, J. *Multi-pass, Single-molecule nanopore Reading of Long Protein Strands with Single-amino Acid Sensitivity.* 2023, BioRxiv, 10−19. DOI: 10.1101/2023.10.19.563182. (accessed 2023−10−26).

(39) Comer, J.; Ho, A.; Aksimentiev, A. Toward Detection of DNA-Bound Proteins Using Solid-State Nanopores: Insights From Computer Simulations. *Electrophoresis* **2012**, *33*, 3466−3479.

(40) Yan, S.; Zhang, J.; Wang, Y.; Guo, W.; Zhang, S.; Liu, Y.; Cao, J.; Wang, Y.; Wang, L.; Ma, F.; et al. Single Molecule Ratcheting Motion of Peptides in a Mycobacterium Smegmatis Porin A (MspA) Nanopore. *Nano Lett* **2021**, *21*, 6703−6710.

(41) Kesselheim, S.; Müller, W.; Holm, C. Origin of Current Blockades in Nanopore Translocation Experiments. *Phys. Rev. Lett.* **2014**, *112*, 018101.

(42) Si, W.; Aksimentiev, A. Nanopore Sensing of Protein Folding. *ACS Nano* **2017**, *11*, 7091−7100.

(43) Wilson, J.; Sarthak, K.; Si, W.; Gao, L.; Aksimentiev, A. Rapid and Accurate Determination of Nanopore Ionic Current Using a Steric Exclusion Model. *ACS Sens* **2019**, *4*, 634−644.

(44) Di Muccio, G.; Rossini, A. E.; Di Marino, D.; Zollo, G.; Chinappi, M. Insights into Protein Sequencing with an α-Hemolysin Nanopore by Atomistic Simulations. *Sci. Reports* **2019**, *9*, 6440.

(45) Golla, V. K.; Prajapati, J. D.; Kleinekathöfer, U. Millisecond-long Simulations of Antibiotics Transport through Outer Membrane Channels. *J. Chem. Theory Comput.* **2021**, *17*, 549−559.

(46) Phillips, J. C.; Hardy, D. J.; Maia, J. D. C.; Stone, J. E.; Ribeiro, J. V.; Bernardi, R. C.; Buch, R.; Fiorin, G.; Henin, J.; Jiang, W.; McGreevy, R.; Melo, M. C. R.; Radak, B. K.; Skeel, R. D.; Singharoy, A.; Wang, Y.; Roux, B.; Aksimentiev, A.; Luthey-Schulten, Z.; Kale, L. V.; Schulten, K.; Chipot, C.; Tajkhorshid, E. Scalable Molecular Dynamics on CPU and GPU Architectures with NAMD. *J. Chem. Phys.* **2020**, *153*, 044130.

(47) Hart, K.; Foloppe, N.; Baker, C. M.; Denning, E. J.; Nilsson, L.; MacKerell, A. D. Optimization of the CHARMM Additive Force Field for DNA: Improved Treatment of the BI/BII Conformational Equilibrium. *J. Chem. Theory Comput.* **2012**, *8*, 348−362.

(48) Huang, J.; MacKerell, A. D., Jr CHARMM36 All-atom Additive Protein Force Field: Validation Based on Comparison to NMR Data. *J. Comput. Chem.* **2013**, *34*, 2135−2145.

(49) Klauda, J. B.; Venable, R. M.; Freites, J. A.; O'Connor, J. W.; Tobias, D. J.; Mondragon-Ramirez, C.; Vorobyov, I.; MacKerell, A. D.; Pastor, R. W. Update of the CHARMM All-Atom Additive Force Field for Lipids: Validation on Six Lipid Types. *J. Phys. Chem. B* **2010**, *114*, 7830−7843.

(50) Jorgensen, W. L.; Chandrasekhar, J.; Madura, J. D.; Impey, R. W.; Klein, M. L. Comparison of Simple Potential Functions for Simulating Liquid Water. *J. Chem. Phys.* **1983**, *79*, 926−935.

(51) Beglov, D.; Roux, B. Finite Representation of an Infinite Bulk System: Solvent Boundary Potential for Computer Simulations. *J. Chem. Phys.* **1994**, *100*, 9050−9063.

(52) Yoo, J.; Aksimentiev, A. Improved Parametrization of Li$^+$, Na$^+$, K$^+$, and Mg^{2+} Ions for All-Atom Molecular Dynamics Simulations of Nucleic Acid Systems. *J. Phys. Chem. Lett.* **2012**, *3*, 45−50.

(53) Yoo, J.; Aksimentiev, A. Improved Parameterization of Amine−Carboxylate and Amine−Phosphate Interactions for Molecular Dynamics Simulations Using the CHARMM and AMBER Force Fields. *J. Chem. Theory Comput.* **2016**, *12*, 430−443.

(54) Yoo, J.; Aksimentiev, A. New Tricks for Old Dogs: Improving the Accuracy of Biomolecular Force Fields by Pair-specific Corrections to Non-bonded Interactions. *Phys. Chem. Chem. Phys.* **2018**, *20*, 8432−8449.

(55) Andersen, H. C. RATTLE: A "Velocity" Version of the SHAKE Algorithm for Molecular Dynamics Calculations. *J. Comput. Phys.* **1983**, *52*, 24−34.

(56) Miyamoto, S.; Kollman, P. A. SETTLE: An Analytical Version of the SHAKE and RATTLE Algorithm for Rigid Water Molecules. *J. Comput. Chem.* **1992**, *13*, 952−962.

(57) Darden, T. A.; York, D. M.; Pedersen, L. G. Particle Mesh Ewald: An N·log(N) Method for Ewald Sums in Large Systems. *J. Chem. Phys.* **1993**, *98*, 10089−10092.

(58) Martyna, G. J.; Tobias, D. J.; Klein, M. L. Constant Pressure Molecular Dynamics Algorithms. *J. Chem. Phys.* **1994**, *101*, 4177−4189.

(59) Brünger, A. T. *X-PLOR, Version 3.1: a System for X-ray Crystallography and NMR*; Yale University Press: New Haven, CT, 1992.

(60) Shaw, D. E.; Grossman, J. P.; Bank, J. A.; Batson, B.; Butts, J. A.; Chao, J. C.; Deneroff, M. M.; Dror, R. O.; Even, A.; Fenton, C. H.; Forte, A.; Gagliardo, J.; Gill, G.; Greskamp, B.; Ho, C. R.; Ierardi, D. J.; Iserovich, L.; Kuskin, J. S.; Larson, R. H.; Layman, T.; et al. Anton 2: Raising the Bar for Performance and Programmability in a Special-Purpose Molecular Dynamics Supercomputer. *IEEE* **2014**, 41−53.

(61) Hoover, W. G. Canonical Dynamics: Equilibrium Phase-Space Distributions. *Phys. Rev. A* **1985**, *31*, 1695−1697.

(62) Shan, Y.; Klepeis, J. L.; Eastwood, M. P.; Dror, R. O.; Shaw, D. E. Gaussian Split Ewald: A fast Ewald Mesh Method for Molecular Simulation. *J. Chem. Phys.* **2005**, *122*, 054101.

(63) Derrington, I. M.; Butler, T. Z.; Collins, M. D.; Manrao, E.; Pavlenok, M.; Niederweis, M.; Gundlach, J. H. Nanopore DNA sequencing with MspA. *Proc. Natl. Acad. Sci. U. S. A.* **2010**, *107*, 16060.

(64) Isralewitz, B.; Izrailev, S.; Schulten, K. Binding Pathway of Retinal to Bacterio-opsin: A Prediction by Molecular Dynamics Simulations. *Biophys. J.* **1997**, *73*, 2972−2979.

(65) Vanommeslaeghe, K.; Raman, E. P.; MacKerell, A. D. Automation of the CHARMM General Force Field (CGenFF) II: Bond Perception and Atom Typing. *J. Chem. Inf. Model.* **2012**, *52*, 3155−3168.

(66) Vanommeslaeghe, K.; MacKerell, A. D. Automation of the CHARMM General Force Field (CGenFF) I: Bond Perception and Atom Typing. *J. Chem. Inf. Model.* **2012**, *52*, 3144−3154.

(67) Feenstra, K. A.; Hess, B.; Berendsen, H. J. Improving Efficiency of Large Time-scale Molecular Dynamics Simulations of Hydrogen-rich Systems. *J. Comput. Chem.* **1999**, *20*, 786−798.